Kinematic characteristics of cam-elliptical gear combined packaged vegetable labeling mechanism

Lei Zhang[1,2], Heng Zhou[1], Chuanyu Wu[3*], Jianneng Chen[1], Xiaowei Zhang[1]

(1. *School of Mechanical Engineering, Zhejiang Sci-Tech University, Hangzhou 310018, China*;
2. *Key Laboratory of Agricultural Equipment for Hilly and Mountainous Areas in Southeastern China (Co-construction by Ministry and Province), Ministry of Agriculture and Rural Affairs, Hangzhou 310018, China*;
3. *School of Marine Engineering Equipment, Zhejiang Ocean University, Zhoushan 316022, Zhejiang, China*)

Abstract: To address the challenges in labeling long labels on curved surface vegetables, such as wrinkles and label detachment, a cam-elliptical gear (C&E) labeling mechanism that realizes an improved hypocycloid trajectory is proposed. Firstly, the influence of different parameters on the hypocycloid trajectory is studied, and the tricuspid hypocycloid is selected as the labeling trajectory. Secondly, the trajectory and kinematic equations of the C&E labeling mechanism with a tricuspid hypocycloid trajectory are established. Next, the influence of various parameters on the trajectory and kinematics of the C&E labeling mechanism is examined. A set of optimal parameters is obtained through a comparative study, and a 3D model of the C&E labeling mechanism is established and simulated. Finally, a prototype of the C&E labeling mechanism was built and experimented with. The experiment showed that the normal labeling completion rate is 94%, and the prototype's efficiency is 56.3 pcs/min. The research in this paper provides a theoretical basis for the design and optimization of a vegetable long-label curved-surface labeling mechanism.

Keywords: hypocycloid, cam-elliptical gear combined mechanism, tricuspid hypocycloid trajectory, kinematics
DOI: 10.25165/j.ijabe.20261903.9152

Citation: Zhang L, Zhou H, Wu C Y, Chen J N, Zhang X W. Kinematic characteristics of cam-elliptical gear combined packaged vegetable labeling mechanism. Int J Agric & Biol Eng, 2026; 19(3): 172–179.

1 Introduction

Vegetable production is becoming increasingly industrialized[1]. Unmanned plant factories are evolving into high-tech facilities characterized by large-scale production and widespread technological adoption[2-4]. Labeling mechanisms play an important role in the packaging of unmanned plant factories. Currently, the widely preferred labeling equipment includes blow-type and bottle labeling mechanisms, which cannot meet the long-label labeling needs of curved-surface vegetables.

In terms of the application of the hypocycloid trajectory, Sirkett et al.[5,6] adopted a planetary gear train with a hypocycloid trajectory for box picking. Tong et al.[7] developed a mechanism combining elliptical and circular gears, which was implemented for box-picking applications. Regarding the epicycloid, Du et al.[8] developed a 5R epicycloid trajectory excitation mechanism specifically for camellia fruit harvesting. Hsu et al.[9] developed a three-link robotic mechanism with two degrees of freedom capable of flexibly generating various hypocycloid and epicycloid curves. Regarding the gear mechanisms, Robison et al.[10] optimized cycloidal gear parameters by employing a genetic algorithm, and Lin et al.[11] replaced cam-driven mechanisms with non-circular gears in the design of in-pipe robots. Although these studies offer valuable design insights, they do not directly address the trajectory requirements necessary for labeling on curved vegetable surfaces.

In this paper, the C&E mechanism is used to label the curved surfaces of vegetables. The specific research contents are as follows: the tricuspid hypocycloid was identified as the labeling trajectory; an improved tricuspid hypocycloid trajectory was proposed; and the improved parametric equation of the tricuspid hypocycloid was established. Then, a C&E labeling mechanism with an improved hypocycloid trajectory was proposed. The kinematic model of the C&E labeling mechanism with an improved hypocycloid trajectory was established, and the final parameters were determined through parameter comparison. Based on the optimized parameters, a prototype of the C&E mechanism is developed. The effectiveness of the mechanism is verified by experiment.

2 Materials and methods

2.1 Study on the labeling process and hypocycloid trajectories

2.1.1 Operation of the cam-elliptical gear integrated labeling mechanism

A C&E labeling mechanism was proposed for surface labeling in unmanned plant factories, which is shown in Figure 1b. The primary structure of the mechanism consists of an elliptical and circular gear planetary gear train arranged symmetrically at 120° intervals. The idler gear and planetary gear are mounted on the rotating bracket. The labeling actuator is secured to the planetary gear shaft, and suction cups are positioned at the left, middle, and

Received date: 2024-06-15 **Accepted date:** 2026-04-15
Biographies: Lei Zhang, Professor, research interest: innovative design of agricultural machinery, Email: lzhang@zstu.edu.cn; **Heng Zhou**, ME, research interest: innovative design of agricultural machinery, Email: 88976963@qq.com; **Jianneng Chen**, Professor, research interest: innovative design of agricultural machinery, Email: jiannengchen@zstu.edu.cn; **Xiaowei Zhang**, ME, research interest: innovative design of agricultural machinery, Email: zhang9801@foxmail.com.
***Corresponding author: Chuanyu Wu**, Professor, research interest: innovative design of agricultural machinery. Faculty of Mechanical Engineering & Automation, Zhejiang Sci-Tech University, Hangzhou 310018, China. Tel: +86-571-86843352, Email: cywu@zstu.edu.cn.

right ends of the labeling actuator. Rotation of the bracket causes the idler gear to rotate around the sun gear. The idler gear then transmits power to the planetary gear, which in turn drives the labeling actuator.

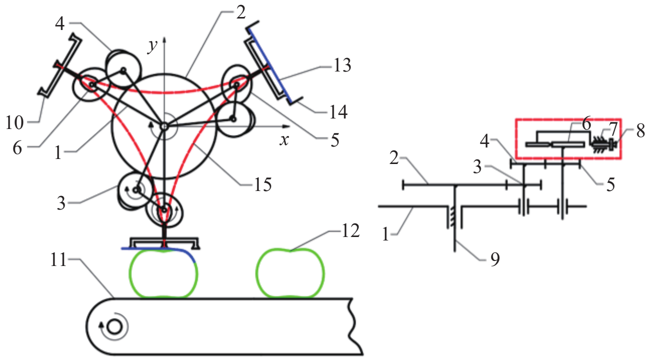

a. The labeling process b. C&E labeling mechanism

1. Rotating bracket 2. Sun gear 3. Circular idler gear 4. Elliptical idler gear 5. Elliptical planetary gear 6. Cam 7. Cam lever 8. Suction cup 9. Fixed shaft 10. Labeling actuator mechanism 11. Conveyor 12. Label object 13. Label 14. Label carrier

Figure 1 Labeling process of the C&E labeling mechanism

The labeling process is as shown in Figure 1a, and it can be described as follows: First, the suction cups on the labeling mechanism secure a label. The rotating bracket moves clockwise, while the planetary gear train transmission labeling actuator rotates counterclockwise in response to the planetary gear. Upon arrival at the labeling station, the suction cup sequentially applies the label to the outer surface of the object: first to the right, then the middle, and finally the left.

2.1.2 Choice of labeling trajectories

Hypocycloid refers to a moving circle (small circle) tangent to a fixed circle (large circle) to roll without sliding, moving a point on the circle around the trajectory[12], as shown in Figure 2. The trajectory can be expressed as:

$$\begin{cases} x=(R_1-r_2)\cos\theta+r_2\cos\left(\dfrac{R_1-r_2}{r_2}\theta\right) \\ y=(R_1-r_2)\sin\theta+r_2\sin\left(\dfrac{R_1-r_2}{r_2}\theta\right) \end{cases} \tag{1}$$

where, R_1 denotes the radius of the large circle, mm; r_2 represents the radius of the small circle, mm; and θ indicates the angle between the center line O_1O_2 and the x-axis, (°).

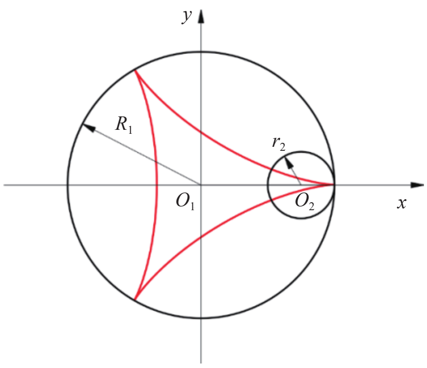

Figure 2 Hypocycloid trajectory

The primary factors influencing the shape of the basic hypocycloid trajectory are the radii of the large and small circles. Figure 3 illustrates the resulting hypocycloid trajectories when the radius of the large circle (R) is two, three, and four times that of the small circle (r), respectively.

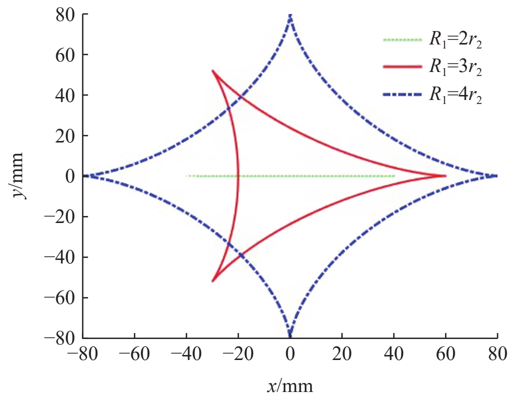

Figure 3 Three types of hypocycloid trajectories

(1) When R_1 is twice r_2, the trajectory is linear. It is not suitable for the curved labeling mechanism designed.

(2) When R_1 is three times of r_2, it is a tricuspid trajectory. The tricuspid trajectory allows three sets of actuators to operate at a cycle time, thereby improving labeling efficiency. Whether in the picking station or the labeling station, the labeling mechanism can be entered at a nearly vertical angle to ensure the accuracy and efficiency of the operation, making it more suitable for labeling applications.

(3) When R_1 is four times of r_2, it is a rhombic trajectory. The rhombic trajectory is not suitable because the actuator cannot be close to the vertical line between the picking point and labeling point.

In many studies, the physical properties of cycloidal curves have been described[13], which also provides a reference for determining the type of curve in this article. In summary, the tricuspid trajectory offers significantly better motion smoothness than the linear or rhombic trajectories, while maintaining the same mechanism simplicity, making it more suitable for continuous labeling.

2.2 Model of cam-elliptical gear combined labeling mechanism

2.2.1 Mathematical model of cam-elliptical gear labeling mechanism

The structure diagram of the C&E labeling mechanism is shown in Figure 4. The symbols in the figure are defined as listed in Table 1.

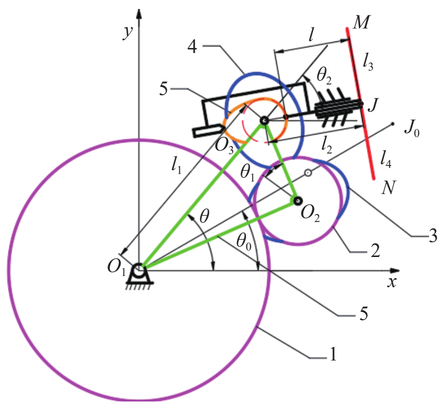

1. Sun gear 2. Circular idler gear 3. Elliptical idler gear 4. Elliptical planetary gear 5. Cam 6. Rotating bracket

Figure 4 Structural diagram of the C&E labeling mechanism

Take O_1 as the origin, take the horizontal direction to the right of the origin as the positive direction of the x-axis, and the vertical direction to the y-axis as the positive direction of the origin, and establish a rectangular coordinate system. The three conditions for J point to form a tricuspid hypocycloidal trajectory are: the ratio of pitch circle radius of sun gear, idler gear, and planetary gear is 3:1:1.

Table 1 Parameter definitions

Name	Definition
O_1	Center of the sun gear
O_2	Center of the idler gear
O_3	Center of the elliptical planetary gear
J	Center point of the middle sucker of the labeling actuator
M	Center point of the right sucker of the labeling actuator
N	Center point of the left sucker of the labeling actuator
J_0	Center point of the sucker after the end of the labeling actuator is displaced after O_1O_3 rotation
l	Distance from the intersection of the concentric lines of O_3 and J and the base circle of the cam to J
l_1	Distance between the solar gear center O_1 and the planetary gear center O_3
l_2	Distance between the planetary gear center O_3 and point J
l_3	Distance between the center point J of the middle sucker and the center point M
l_4	Distance between the center point J of the middle sucker and the center point N
θ_0	Initial angle between O_1O_3 and the x-axis
θ_1	The angle of the idler gear
θ_2	The angle of the elliptical planetary gear
σ_1	The angle between the short half axis of the elliptical idler gear and O_2O_3

The initial angle between O_1O_3 and the x-axis is $\pi/6$; the elliptical idler gear is the same size as the elliptical planetary gear. Therefore, when the rotating bracket rotates, the elliptical planetary gear will rotate, causing the suction cup to rotate from point J to J_0.

The displacement equation of the center point J of the elliptical-circular gear planetary gear train is established:

$$\begin{cases} x = l_1\cos\theta + l_2\cos(\theta-\theta_2) \\ y = l_1\sin\theta + l_2\sin(\theta-\theta_2) \end{cases} \quad (2)$$

The point M displacement equation:

$$\begin{cases} x = l_1\cos\theta + l_2\cos(\theta-\theta_2) - l_3\cos(\theta-\theta_2) \\ y = l_1\sin\theta + l_2\sin(\theta-\theta_2) + l_3\sin(\theta-\theta_2) \end{cases} \quad (3)$$

The point N displacement equation:

$$\begin{cases} x = l_1\cos\theta + l_2\cos(\theta-\theta_2) + l_4\cos(\theta-\theta_2) \\ y = l_1\sin\theta + l_2\sin(\theta-\theta_2) - l_4\sin(\theta-\theta_2) \end{cases} \quad (4)$$

where, α is the independent variable of the angle of the elliptical idler gear, θ_2 is the angle of the elliptical planetary gear relative to O_2O_3, and its expression is as follows:

$$\theta_2 = \int_{\sigma_1}^{\sigma_1+\theta_1} i_{21}\mathrm{d}\alpha \quad (5)$$

where, i_{21} is the transmission ratio of the elliptical gear, and its expression is as follows:

$$i_{21} = \frac{1-e^2}{1+2e\cos\alpha+e^2} \quad (6)$$

where, e is the eccentricity of the elliptical gear, and its expression is as follows:

$$e = \frac{c}{a} \quad (7)$$

where, a is the short half-shaft of the elliptical gear, mm; c is half of the focal distance of the elliptical gear, mm.

As can be seen from Figure 4, the trajectory equation of the point J of the C&E mechanism is as follows:

$$\begin{cases} x = l_1\cos\theta + (l+s)\cos(\theta-\theta_2) \\ y = l_1\sin\theta + (l+s)\sin(\theta-\theta_2) \end{cases} \quad (8)$$

where, s is the motion equation of the cam. The distance l_2 between the center of the planetary gear and the center point J, which is equal to l plus s, changes with the displacement of the cam push rod, and the change range is [$l_{2\min}$, $l_{2\max}$]. Where $l_{2\min}$ represents the distance between the cam center and the point J when the cam push rod is about to be pushed travel; $l_{2\max}$ represents the distance when the cam push rod is about to make a return travel.

2.2.2 Kinematic modeling of a cam-elliptical gear combined labeling mechanism

As can be seen from Equation (8), when l_1, l, and h of the C&E labeling mechanism are determined, the trajectory of point J is determined solely by the rotation angle. The rotation speed of the rotating bracket is set at 20 rad/min. The kinematics equation of the point J can be obtained as follows:

$$\begin{cases} v_x = -2/3\pi l_1\sin(2/3\pi t) - (l+s)\sin(2/3\pi t-\theta_2)\cdot \\ \quad (2/3\pi+\dot{\theta}_2) + \dot{s}\cos(2/3\pi t-\theta_2) \\ v_y = 2/3\pi l_1\cos(2/3\pi t) + (l+s)\cos(2/3\pi t-\theta_2)\cdot \\ \quad (2/3\pi+\dot{\theta}_2) + \dot{s}\sin(2/3\pi t-\theta_2) \end{cases} \quad (9)$$

where, θ_2 is the angle of elliptical planetary gear relative to O_2O_3, $\dot{\theta}_2$ is the angular velocity of the elliptical planetary gear, and $\dot{s}$ is the derivative of s. The expression for both is as follows:

$$\theta_2 = \int_0^{2\pi t-\frac{\pi}{2}} \frac{-(e^2-1)}{e^2+2e\cos\alpha+1}\mathrm{d}\alpha \quad (10)$$

$$\dot{\theta}_2 = \frac{2\pi(e^2-1)}{e^2+2e\cos\left(2\pi t-\frac{\pi}{2}\right)+1} \quad (11)$$

The combined speed is:

$$v = \sqrt{v_x^2+v_y^2} \quad (12)$$

2.3 Research on kinematics characteristics of C&E mechanism

It can be concluded that when l_1, l, h, and e are determined, the motion trajectory of the point J is a function of θ. The trajectory of the point J is symmetrical. Only the influence of l_1, l, h, and e on the motion trajectory of the point J should be considered. For references[7], take l_1 as 120, l as 52, h as 8, and e as 0.1.

2.3.1 Influence of different rod length conditions on the kinematics of the mechanism

When l_1 is greater than twice l plus s, the curve near the cusp is smooth; when l_1 is less than twice l plus s, the curve near the cusp is crossing. By comparing these two cases with the trajectory of l_1 equal to twice l plus s, as shown in Figure 5, it can be seen that when l_1 is equal to twice l plus s, the curve near the cusp is close to the straight line, and the work of picking and labeling the label can be successfully completed.

2.3.2 Influence of different eccentricity ratios on the kinematics of the mechanism

According to the conditions of elliptical gear transmission, the ratio of maximum angle to minimum angle k is not greater than 5[14,15]. Take a as 20, take c as 1, 2, 3, and the corresponding eccentricity ratios of elliptical gear e as 0.05, 0.1, 0.15.

$$k=\left(\frac{a+c}{a-c}\right)^2 \tag{13}$$

The trajectories of the point J are shown in Figure 6.

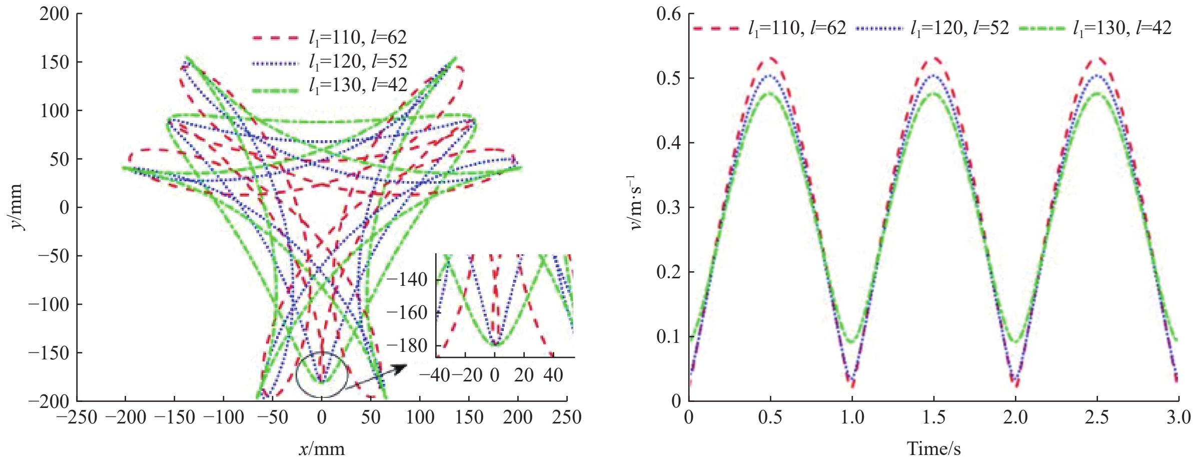

a. Trajectory comparison b. Velocity comparison

Figure 5 Influence of l_1 and l relationship on mechanism

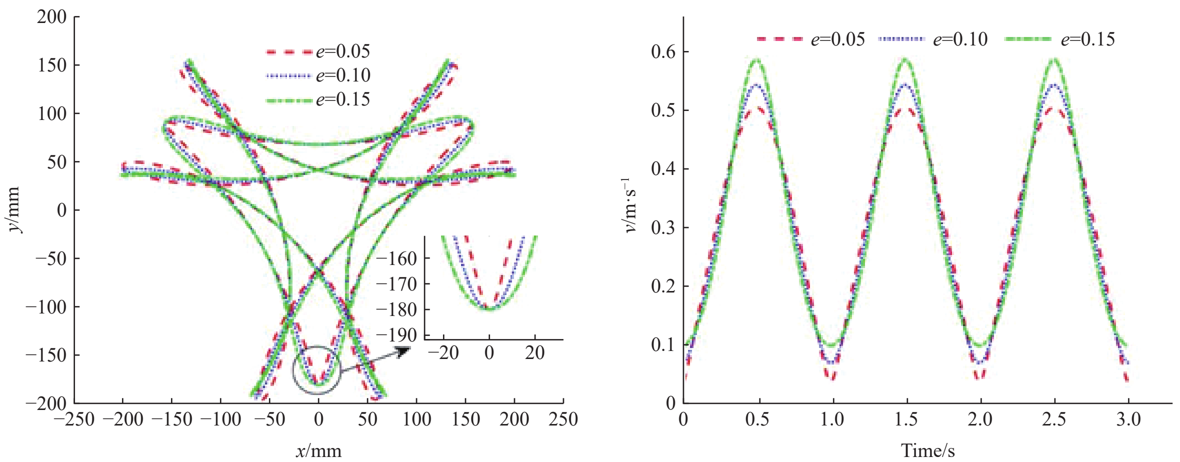

a. Trajectory comparison b. Velocity comparison

Figure 6 Influence of different eccentricity ratios on the mechanism

2.3.3 Influence of different cam motion types on the kinematics of the mechanism

This paper studies the trajectories of the simple harmonic motion cam, the sine acceleration curve cam, and the constant velocity cam. The motion equations are as follows.[16]

$$s=\begin{cases}h[(\delta/\delta_0)-\sin(2\pi\delta/\delta_0)/(2\pi)], & 0\le\delta<\pi\\ h[1-(\delta/\delta_0)+\sin(2\pi\delta/\delta_0)/(2\pi)], & \pi\le\delta\le2\pi\end{cases} \tag{14}$$

$$s_1=\begin{cases}h[1-\cos(\pi\delta/\delta_0)]/2, & 0\le\delta<\pi\\ h[1-\cos(\pi\delta/\delta_0)]/2, & \pi\le\delta\le2\pi\end{cases} \tag{15}$$

$$s_2=\begin{cases}h\delta/\delta_0, & 0\le\delta<\pi\\ h(1-\delta/\delta_0), & \pi\le\delta\le2\pi\end{cases} \tag{16}$$

where, s, s_1, and s_2 represent the motion equations of the simple harmonic, sine acceleration, and constant velocity, respectively; δ is the cam motion angle, δ is equal to θ_2; δ_0 is the cam motion angle, $0\le\delta_0\le180°$ is the return travel, $180°\le\delta_0\le360°$ is the push travel; h is the stroke of the push rod.

The influence of three cam motion curves on the trajectory is shown in Figure 7.

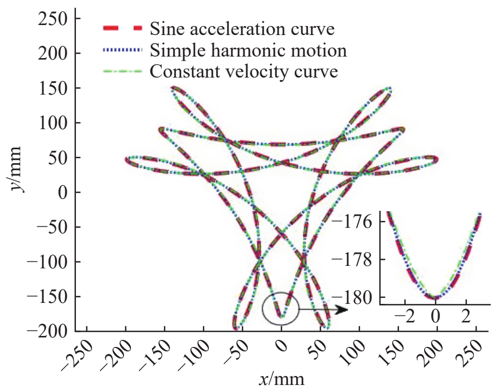

Figure 7 Influence of different cam motion types on the mechanism

3 Results and discussion

3.1 Simulation of cam-elliptical gear labeling mechanism

3.1.1 Analysis of parameter comparison results

After comparative studies, when we take l_1 as 114.5, l as 57.5, l_3 and l_4 as 60, c as 0.05, and a as 22.75, the trajectory near the cusp approaches the plumb line. The speed is approximately 0 m/min, enabling vertical labeling. The sine acceleration curve can exhibit neither rigid nor soft impact during both push and return movements; therefore, the sine acceleration motion is selected. Figure 8 compares parameters before and after the study.

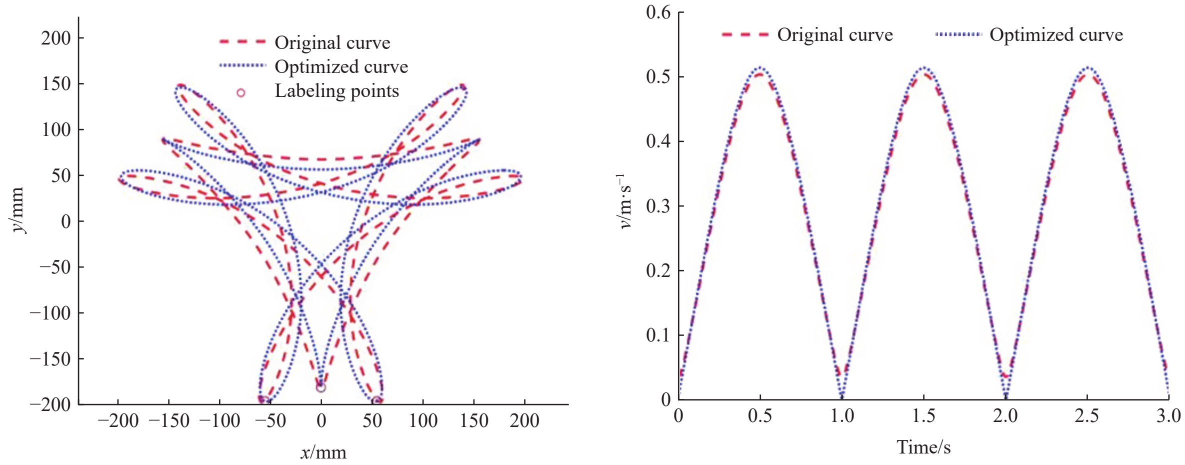

a. Trajectory comparison b. Velocity comparison

Figure 8 Before and after optimization

Based on the process requirements and label dimensions, the X_r coordinate of the labeling starting point is set to (55, –195), the X_m coordinate of the midpoint to (0, –180), and the X_l coordinate of the labeling endpoint to (–55, –195). The total arc length from the starting point through the midpoint to the endpoint is 120 mm. To ensure that the label at point M can be smoothly affixed at the starting point, the distance between the farthest point of point M's trajectory and the labeling starting point is defined as follows:

$$f_1(x) = \min\left(\sqrt{(x_{\max}-x_r)^2+(y_{\max}-y_r)^2}\right) \tag{17}$$

where, $x_{\max}$, $y_{\max}$ is the coordinate of x and y when the value of $f_0(x, y)$ is the maximum, which can be expressed as:

$$\max f_0(x,y) = \sqrt{x_{\max}^2+y_{\max}^2},\quad x>0, y<0 \tag{18}$$

The distance between point M and the labeling starting point Xr is used as one evaluation index. Additionally, $v_{\min}$ serves as another evaluation index, as presented in Table 2.

Table 2 Original curve and optimized curve

	Labeling error distance/mm	$v_{\min}$/m·s^{-1}
Original curve	3.871	0.036
Optimized curve	0.338	9.9×10^{-5}

As can be seen from Table 2, the labeling error distance is reduced from 3.871 to 0.338 mm, and the $v_{\min}$ is reduced from 0.036 to 9.9×10^{-5} m/s. The C&E labeling mechanism has better kinematics characteristics and can achieve the labeling point.

3.1.2 Elliptical gear and cam generation

Based on the established relationship between the eccentricity ratio and the angle of the elliptical gear, the corresponding pitch curve equation can be derived as follows:

$$R_{j1} = \frac{a(1-e^2)}{1+e\cos\theta_2} \tag{19}$$

where, a denotes the major semi-axis of the elliptical gear, mm; e represents the eccentricity ratio of the elliptical gear; and θ_2 indicates the angle of the elliptical gear.

The pitch curve of another elliptical gear can be obtained as follows:

$$R_{j2} = \frac{a(1+2e\cos\theta_2+e^2)}{1+e\cos\theta_2} \tag{20}$$

The transmission ratio of the elliptical gear is:

$$i_{21} = \frac{1-e^2}{1+e^2-2e\cos\theta_2} \tag{21}$$

Profile-generating software for non-circular gears, which employs the generative method[17-19], is used to generate the profiles of elliptical gears.

The process of generating an elliptical gear profile using software involves importing an appropriate pitch curve, calculating the pitch curve using Matlab, saving the resulting scatter points as an .xlsx file, and subsequently loading the file into profile generation software to produce a complete elliptical gear profile. Figure 9 presents the pitch curve and tooth profile of the generated elliptical gear. The profile curve should be examined to confirm that it is closed. If the curve is closed, the profile dataset of the elliptical gear is exported in ".txt" format and subsequently imported into UG 3D modeling software to generate the corresponding 3D model.

The contour of the cam is shown in Figure 10a, and the 3D model is shown in Figure 10b.

3.1.3 Establishment and simulation of C&E labeling mechanism

In SolidWorks, the 3D model of the labeling mechanism is saved as a ".x_t" format file, and the corresponding working path is imported into the Adams software. The 3D model established is shown in Figure 11.

The simulated trajectory is shown in Figure 12.

3.2 Experiment of cam-elliptical gear labeling mechanism

The assembled mechanism prototype is shown in Figure 13. To verify the effectiveness of the C&E labeling mechanism with an improved hypocycloidal trajectory, experimental studies were conducted on the prototype. Experiments were conducted at ambient room temperature (approximately 23°C-25°C). Each packaged vegetable was positioned on the conveyor belt at a fixed 300 mm spacing, with the length of the packaged vegetables oriented perpendicular to the conveyor belt's direction of travel. The conveyor belt transported the packaged vegetables at 300 mm/s.

The damage rate, the normal labeling completed rate, and the efficiency of the prototype are used to evaluate the comprehensive performance of the prototype in the labeling operation. The evaluation method and indices are described as follows:

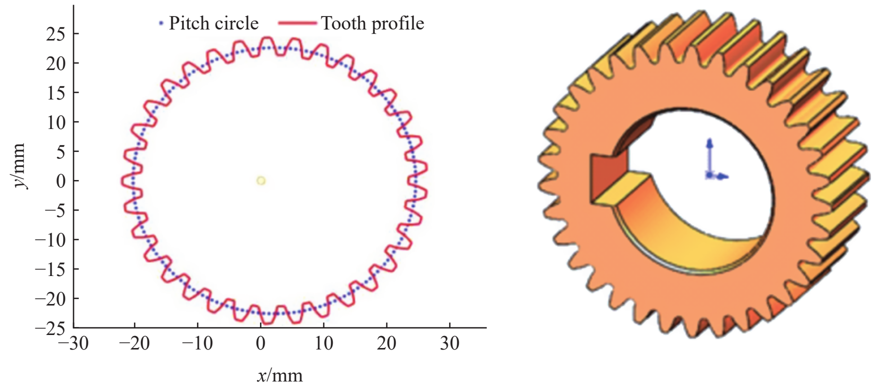

a. Pitch curve and tooth profile of elliptical gear b. 3D model of elliptical gear

Figure 9 Pitch curve and tooth profile of elliptical gear and three-dimensional model

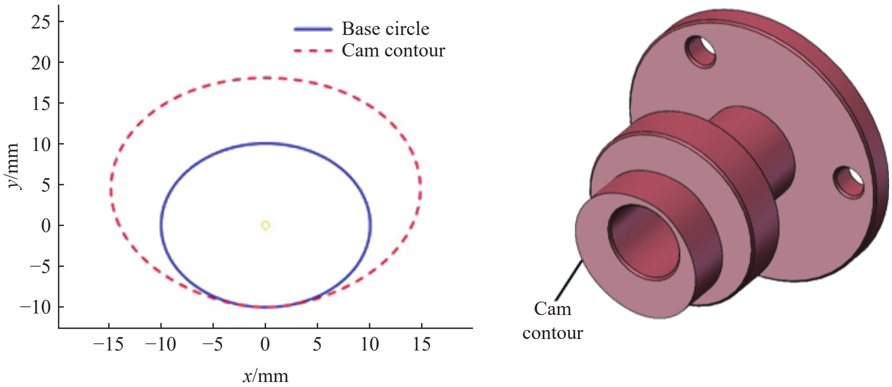

a. Cam contour and base circle b. 3D model of cam

Figure 10 Cam profile and 3D model

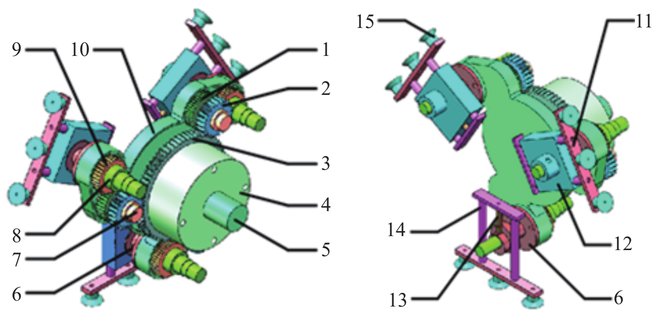

a. Back site b. Front site

1. Elliptical idler gear; 2. Circle idler gear; 3. Sun gear; 4. Sun gear mounting base; 5. Drive shaft; 6. Cam; 7. Intermediate shaft; 8. Planetary shaft; 9. Elliptical planetary gear; 10. Rotating bracket; 11. Sucker mounting rod; 12. Sliding sleeve; 13. Putting rod; 14. Sliding rod; 15. Suction cups

Figure 11 3D model of C&E labeling mechanism

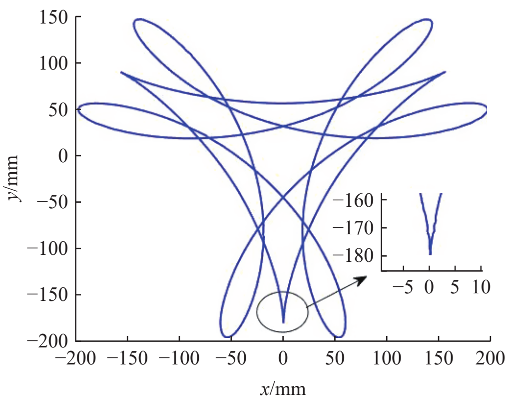

Figure 12 Simulation trajectory

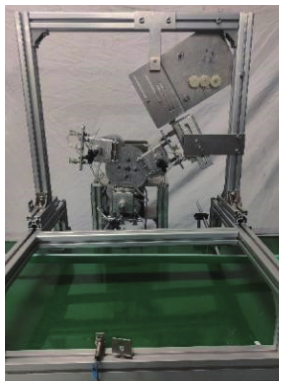

Figure 13 C&E labeling prototype

After labeling, leaf vegetables were sampled to assess the quality of each individually packaged specimen. Labeled damaged leaves were then removed and their quality measured separately. The vegetable damage rate can be calculated as follows:

$$S_c = \frac{C_S}{C_Z} \times 100 \tag{22}$$

where, S_c is the damage rate, %; C_s is the quality of damaged part of packaged vegetable, g; C_z is the total mass of packaged vegetable, g.

The total number of labeled packaged vegetables and the number of normal labeling completed labeled packaged vegetables are recorded. The normal labeling completion rate can be calculated according to the following:

$$M = \frac{M_v}{M_t} \times 100 \tag{23}$$

where, M is the normal labeling completed rate, %; M_v is the number of normal labeling completed labeled packaged vegetables, package; M_t is the total number of labeled packaged vegetables, package.

The efficiency of the prototype can be effectively evaluated by recording the number of normal labels completed in 60 minutes and calculating according to the following:

$$V = \frac{M_v}{T} \tag{24}$$

where, V is the efficiency of the prototype, pcs/min; T indicates the labeling operation time, min.

3.3 Experimental results and analysis

In summary, the C&E labeling prototype was built, and the prototype experiment was conducted. A series of labeling experiments was carried out on vegetables in unmanned plant factories, as shown in Figure 14. It can be seen from Figure 14a and Figure 14b that the labeling prototype is smoother when labeling the right and left sides of the packaged dishes. To further demonstrate the effectiveness of labeling for curved vegetables, the labeling experiment was conducted on curved vegetables (e.g., cabbage).

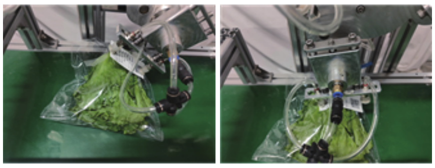

a. Complete labeling on the right side of the lettuce b. Complete labeling on the left side of the lettuce

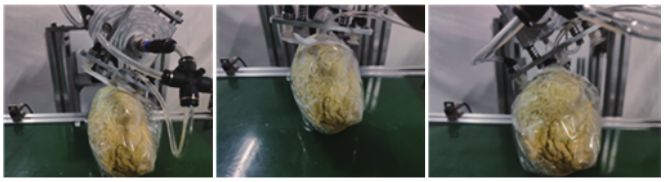

c. Complete the labeling of the right side of the curved vegetable d. Complete the labeling of the up side of the curved vegetable e. Complete the labeling of the left side of the curved vegetable

Figure 14 Labeling process of different vegetables

As can be seen from Figure 14, when the labeling actuator runs to the position shown in Figure 14c, the label on the suction cup of the labeling actuator first contacts the right side of the packaged vegetable. Then, the labeling actuator and conveyor belt continue to run, pasting the middle part of the label shown in Figure 14d. Finally, the label on the left suction cup is attached to the left side of the packaged vegetable shown in Figure 14e. The labeling effect of curved packaged vegetables is shown in Figure 15. From the figure, it can be seen that the label was fully adhered to the surface of the packaged vegetables, with no curling, folding, or damage.

Figure 15 Curved surface vegetable labeling effect

Six groups of experiments were completed, each lasting 1 minute and yielding a throughput of 60 packaged vegetables per minute, for a total sample size of 360. After labeling, samples were collected for evaluation. The experimental evaluation indices were calculated as listed in Table 3.

Table 3 Experimental indices calculation

Num.	Number of labeling failures (Package)	Damage rate/%	Normal labeling completed rate/%	Efficiency of the prototype/(pcs·min^{-1})
1	2	0.1	97	58
2	3	0.2	95	57
3	4	1	93	56
4	5	0.3	92	55
5	2	0.1	97	58
6	6	0.5	90	54
Avg.	3.7	0.2	94	56.3

As shown in Table 3, the average number of failed packages is 3.7, the average damage rate is 0.2%, and the normal labeling completion rate is 94%. The prototype's efficiency is 56.3 pcs/min.

It can be observed that the damage to leafy vegetables is mainly concentrated in the labeling step, and a small amount of damage is caused by direct contact between the sucker and the vegetable. The main reasons for the labeling failure include two main points: Firstly, the packaging bags and vegetables are not tight enough, and the packaging bags easily deform during the labeling process, which affects the labeling quality. Secondly, the negative pressure provided by the air pump during the labeling process is not enough, resulting in the label being unable to be removed from the label tray.

To address the two issues above, corresponding improvements are proposed for future work. For the loose packaging bags, a pre-tensioning mechanism or a soft roller can be installed upstream of the labeling station to gently flatten the bag surface before labeling. Alternatively, reducing the conveyor speed or applying a slight vacuum under the bag can enhance stability. To compensate for insufficient negative pressure, a higher-capacity vacuum pump with a pressure stabilizer or a closed-loop pressure control system can be used to maintain consistent suction at the suction cup. Moreover, using larger-diameter suction cups or porous foam suction cups may improve adhesion on uneven bag surfaces. These proposed measures are expected to further reduce the labeling failure rate and improve overall reliability in future prototype iterations.

4 Conclusions

(1) To address the curved-surface labeling problem for packaged vegetables in unmanned plant factories, the tricuspid hypocycloid was identified as the labeling trajectory, and an improved tricuspid hypocycloid trajectory was proposed, along with the corresponding parametric equation.

(2) To address the problem of accurate labeling of packaged vegetables in unmanned plant factories, a C&E labeling mechanism with an improved hypocycloidal trajectory was proposed. A kinematic model of the C&E labeling mechanism with an improved hypocycloidal trajectory was established, and the final parameters were determined by parameter comparison.

(3) The 3D model of the elliptical gear and cam of the mechanism is established, and the whole mechanism is assembled. Adams software is used to simulate and analyze the mechanism, and the point J trajectory is obtained. By comparison, it is found to be generally consistent with the theoretical trajectory, which confirms the correctness of the theoretical design.

(4) After the experimental study, the average number of failed packets for the labeling mechanism is 3.7, the average damage rate for leafy vegetables is 0.2%, and the normal labeling completion

rate is 94%. The prototype's efficiency is 56.3 pcs/min. The experimental results show that the developed C&E labeling mechanism can meet the demands of an actual vegetable unmanned factory.

Acknowledgements

This work was supported by the National Key Research and Development China Project (Grant No. 2021YFD2000700). Any opinions, findings, conclusions, or recommendations expressed in this publication are those of the authors and do not necessarily reflect the view of Zhejiang Sci-Tech University.

[References]

[1] Chen K, Yuan Y, Zhao B, Zhou L, Niu K, Jin X, et al. Digital twins and data-driven in plant factory: An online monitoring method for vibration evaluation and transplanting quality analysis. Agriculture, 2023; 13(6): 1165.

[2] Zhang Y, Kacira M. Analysis of climate uniformity in indoor plant factory system with computational fluid dynamics (CFD). Biosyst. Eng., 2022; 220: 73–86.

[3] Jin X, Tang L M, Li R, Zhao B, Ji T, Ma Y, et al. Edge recognition and reduced transplantation loss of leafy vegetable seedlings with Intel RealsSense D415 depth camera. Comput. Electron. Agric., 2022; 198: 107030.

[4] Jin X, Tang L M, Li R, Ji J, Liu J. Selective transplantation method of leafy vegetable seedlings based on ResNet 18 network. Front. Plant Sci., 2022; 13: 893357.

[5] Sirkett D M, Hicks B J, Berry C, Mullineux G, Medlandal A. Finite element simulation of folding carton erection failure. Proceedings of the Institution of Mechanical Engineers, Part C: Journal of Mechanical Engineering Science, 2007; 221(7): 753–767. DOI: 10.1243/0954406JMES502

[6] Sirkett D M, Hicks B J, Berry C, Mullineux G, Medlandal A. Simulating the behaviour of folded cartons during complex packing operations. Proc. Inst. Mech. Eng. Part C-J. Eng. Mech. Eng. Sci., 2006; 220(12): 1797–1811.

[7] Tong J H,Tang Q Q, Wu C Y, Lou H F, Cheng P L, Li X. Elliptical-circular planetary gear train box-taking mechanism design and trajectory analysis for automatic cartoning mechanisms. Chin. J. Mech. Eng., 2018; 54(11): 172. (In Chinese)

[8] Du X Q, Han X T, Shen T F, Li S T, He L Y. Design and experiment of two-degree-of-freedom canopy shaking equipment based on 5R parallel mechanism. Transactions of the CSAM, 2023; 54(4): 96–106. (in Chinese)

[9] Hsu M H, Tsai Z Y, Hsieh L C, Liu J Y. On the design of three links robot for drawing epicycloid and hypocycloid curves. Advanced Energy Systems, Advanced Materials, Aerospace, Automation and Robotics, Noise Control and Acoustics, and Systems Engineering, 2006; pp.783-789. DOI: 10.1115/ESDA2006-95546.

[10] Robison A J, Vacca A. Performance comparison of epitrochoidal, hypotrochoidal, and cycloidal gerotor gear profiles. Mech. Mach. Theory, 2021; 158: 104228.

[11] Lin C, Hu Y, Wei Y, Cai Z. Characteristics analysis of supporting and locking mechanism based on the non-circular gear compound transmission. J. Mech. Sci. Technol., 2020; 34(6): 2561–2571.

[12] Dion-Gauvin P, Gosselin C. Dynamic point-to-point trajectory planning of a three-DOF cable-suspended mechanism using the hypocycloid curve. IEEE-ASME Trans. Mechatron, 2018; 23(4): 1964–1972.

[13] Wang B, Geng Y, Chu J. Generation and application of hypocycloid and astroid. Journal of Physics: Conference Series, 2019; 1345(3): 032085.

[14] Bair B W. Computer aided design of elliptical gears with circular-arc teeth. Mech. Mach. Theory, 2004; 39(2): 153–168.

[15] Li G, Zhu W. Design and power loss evaluation of a noncircular gear pair for an infinitely variable transmission. Mech. Mach. Theory, 2021; 156: 104137.

[16] Pazarkaya İ, Yazar M, Özdemir A. Computational fluid dynamics analysis of flowmeters with elliptical gear pairs and evaluation of calculated flow rate by Taguchi method. Flow Meas. Instrum, 2023; 94: 102476.

[17] Podgornyj Y, Skeeba V, Kirillov A, Martyushev N, Borisov M. The synthesis of motion laws for cam mechanisms with additional movement of the follower. IOP Conference Series: Earth and Environmental Science, 2019; 378: 012025.

[18] Sharma A, Khar S. Design and development of a vegetable plug seedling transplanting mechanism for a semi-automatic transplanter. Sci. Hortic., 2024; 326: 112773. DOI: 10.1016/j.scienta.2023.112773

[19] Zhao H, Chen J, Xu G. Design methodology and characteristics analysis of high-order multi-segment deformed eccentric non-circular gear. Facta Universitatis, Series: Mechanical Engineering, 2024; 22(2): 217–234.